

Radiation-Induced Helium Nanobubbles Enhance Ductility in Submicron-Sized Single-Crystalline Copper

Ming-Shuai Ding,[†] Jun-Ping Du,[‡] Liang Wan,^{†,‡} Shigenobu Ogata,^{‡,§} Lin Tian,[†] Evan Ma,^{†,||} Wei-Zhong Han,^{*,†} Ju Li,^{*,†,⊥} and Zhi-Wei Shan[†]

[†]Center for Advancing Materials Performance from the Nanoscale & Hysitron Applied Research Center in China, State Key Laboratory for Mechanical Behavior of Materials, Xi'an Jiaotong University, Xi'an 710049, P.R. China

[‡]Department of Mechanical Engineering and Bioengineering, Osaka University, Osaka 565-0871, Japan

[§]Center for Elements Strategy Initiative for Structural Materials, Kyoto University, Kyoto 606-8501, Japan

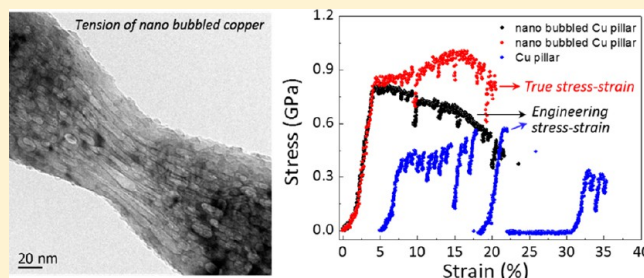
^{||}Department of Materials Science and Engineering, Johns Hopkins University, Baltimore, Maryland 21218, United States

[⊥]Department of Nuclear Science and Engineering and Department of Materials Science and Engineering, Massachusetts Institute of Technology, Cambridge, Massachusetts 02139, United States

Supporting Information

ABSTRACT: The workability and ductility of metals usually degrade with exposure to irradiation, hence the phrase “radiation damage”. Here, we found that helium (He) radiation can actually enhance the room-temperature deformability of submicron-sized copper. In particular, Cu single crystals with diameter of 100–300 nm and containing numerous pressurized sub-10 nm He bubbles become stronger, more stable in plastic flow and ductile in tension, compared to fully dense samples of the same dimensions that tend to display plastic instability (strain bursts). The sub-10 nm He bubbles are seen to be dislocation sources as well as shearable obstacles, which promote dislocation storage and reduce dislocation mean free path, thus contributing to more homogeneous and stable plasticity. Failure happens abruptly only after significant bubble coalescence. The current findings can be explained in light of Weibull statistics of failure and the beneficial effects of bubbles on plasticity. These results shed light on plasticity and damage developments in metals and could open new avenues for making mechanically robust nano- and microstructures by ion beam processing and He bubble engineering.

KEYWORDS: Radiation damage, He bubble, ductility, in situ TEM, submicron-sized



The mechanical behaviors of metals are usually designed for bulk applications, but in the past few decades, numerous microscale and nanoscale applications have emerged.¹ These small-volume metal (with sample size less than 1 μm) parts need to be mechanically robust enough to serve their functions. The mechanical properties of small-volume materials are largely different from their bulk counterpart, due to size-effect on plasticity and fracture. At room temperature, once the sample dimension shrinks below a few microns, they generally become stronger, less controllable in plastic deformation and reach ultimate failure faster and less predictably.^{1–9} It would be very beneficial to develop scalable material processing method to improve the formability and ductility (mechanical energy absorption) of small-volume metals.

Ion beam processing is already indispensable in micro- and nanotechnologies.¹⁰ However, the possible adverse effect of ion radiation on mechanical properties of small-volume materials is a major concern.^{11–14} The degradation effects of neutron and ion radiations on mechanical properties of bulk metals are well-documented, based on experiences with bulk structural

materials in nuclear fission and fusion reactors.^{10–14} In particular, He bubbles accumulate inside bulk metals, especially along sinks such as dislocations, precipitates and grain boundaries, resulting in reduction of bonded area and leading to macroscopic embrittlement.^{11–14} Recent nanomechanical studies on He-implanted metals indicated that He bubbles also strongly affect the plastic deformation of small-volume metals.^{15–20} In the present work, based on systematic in situ nanomechanical experiments, we found that the implanted nanoscale He bubbles benefit dislocation storage while reducing dislocation mean free path, and lead to the enhanced ductility of submicron-sized copper single crystal, contrary to the general concept that radiation will deteriorates the plastic deformation ability of materials.

We first implanted 200 keV He ions into well-annealed Cu at 450 °C to a fluence of 2×10^{17} ions cm^{-2} .²¹ Due to the very

Received: February 28, 2016

Revised: April 5, 2016

Published: June 1, 2016

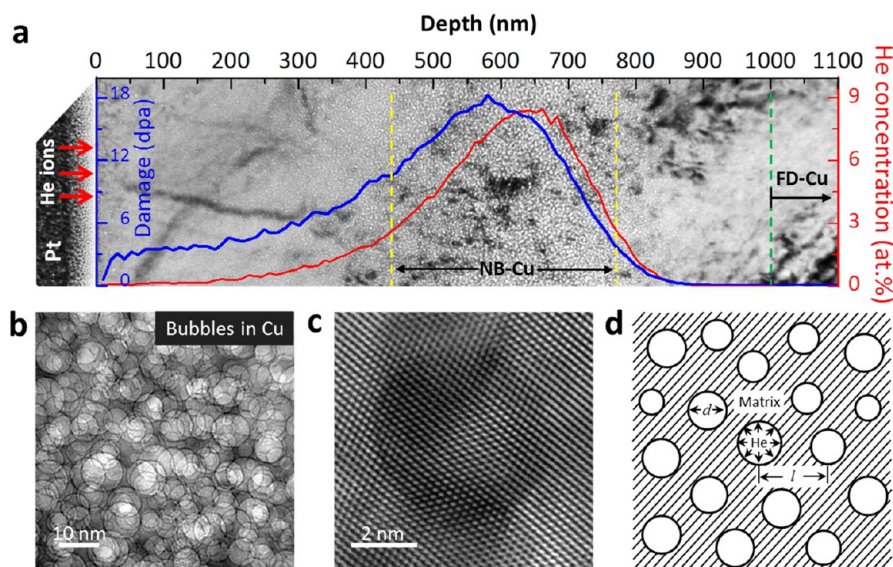


Figure 1. Microstructure of nano-bubbled metals. (a) The variation of He bubble distribution and damage with the depth from the surface. (b) Typical transmission electron microscopy image of the He implanted copper cut from the region marked by yellow dashed lines in a. (c) The high resolution image of a single He bubble. (d) Schematic illustration of the typical microstructural feature of NB-Cu, which is a bubble–copper composite.

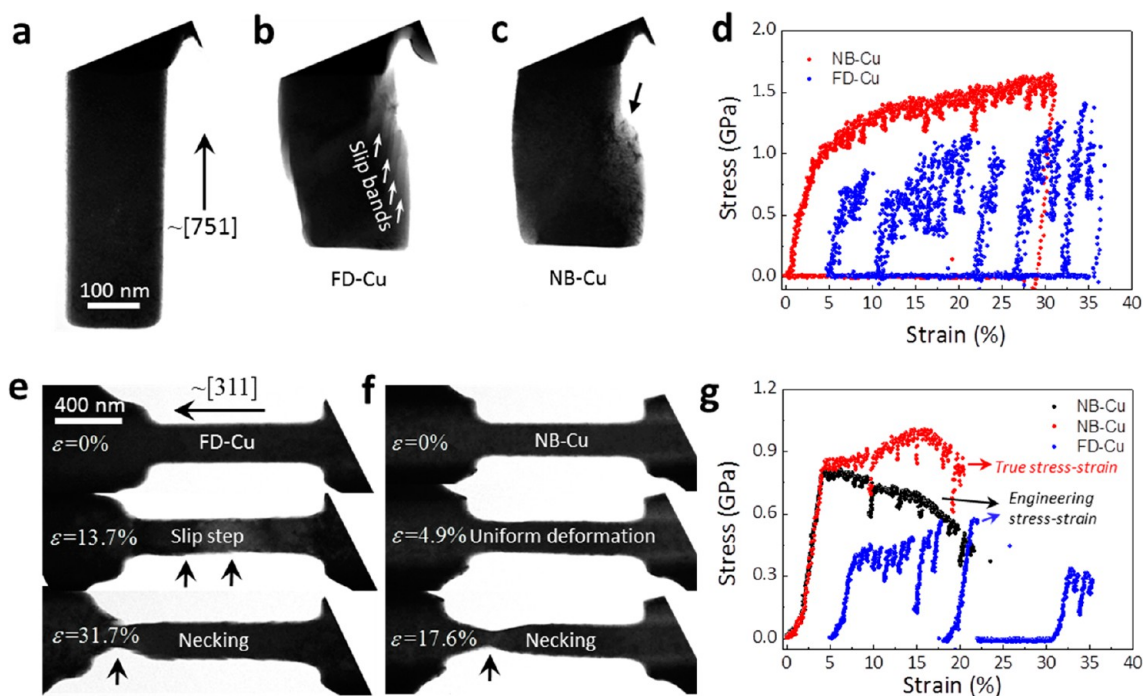


Figure 2. Compressive and tensile behavior of the fully dense and nano bubbled Cu single crystal pillars. (a) Rectangle pillar with [751] orientation for in situ compressive test. (b and c) Postcompression images of the FD-Cu and NB-Cu single crystal pillars. Obvious sharp slip bands marked by white arrows are formed on FD-Cu pillar (b), while only smooth deformation profile is observed on NB-Cu pillar (c). (d) Engineering stress–strain curve of the FD-Cu and NB-Cu single crystal pillars. (e) Tensile deformation of FD-Cu pillars with loading axis near [311]. (f) Tensile deformation of NB-Cu pillars with loading axis near [311]. (g) Engineering/true stress–strain curve of FD-Cu and NB-Cu single crystal pillars. NB-Cu started to necking at strain of 7%. The blue curves in d and g were shifted intentionally for better legibility.

low solubility in metals, He coprecipitated out with radiation-generated vacancies to form nanoscale He bubbles. These bubbles are expected to be near equilibrium condition (He bubble pressure balancing with the internal surface energy) due to the slow cooling after high temperature implantation.²¹ The radiation damage (in unit of displacements per atom (dpa), blue) and He distribution (red) can be estimated by Monte

Carlo simulation,²² as shown in Figure 1a. The predicted He distribution agrees well with the observed He bubble density. We then machined out submicron-sized samples by focus ion beam, away from grain boundaries in the single-crystalline region, with sample diameter D ($D \equiv \sqrt{A}$, where A is the cross-section area of the tested samples) ranging from 100 to 300 nm, at a depth with 3–8 atom % He implanted. Figures 1b and

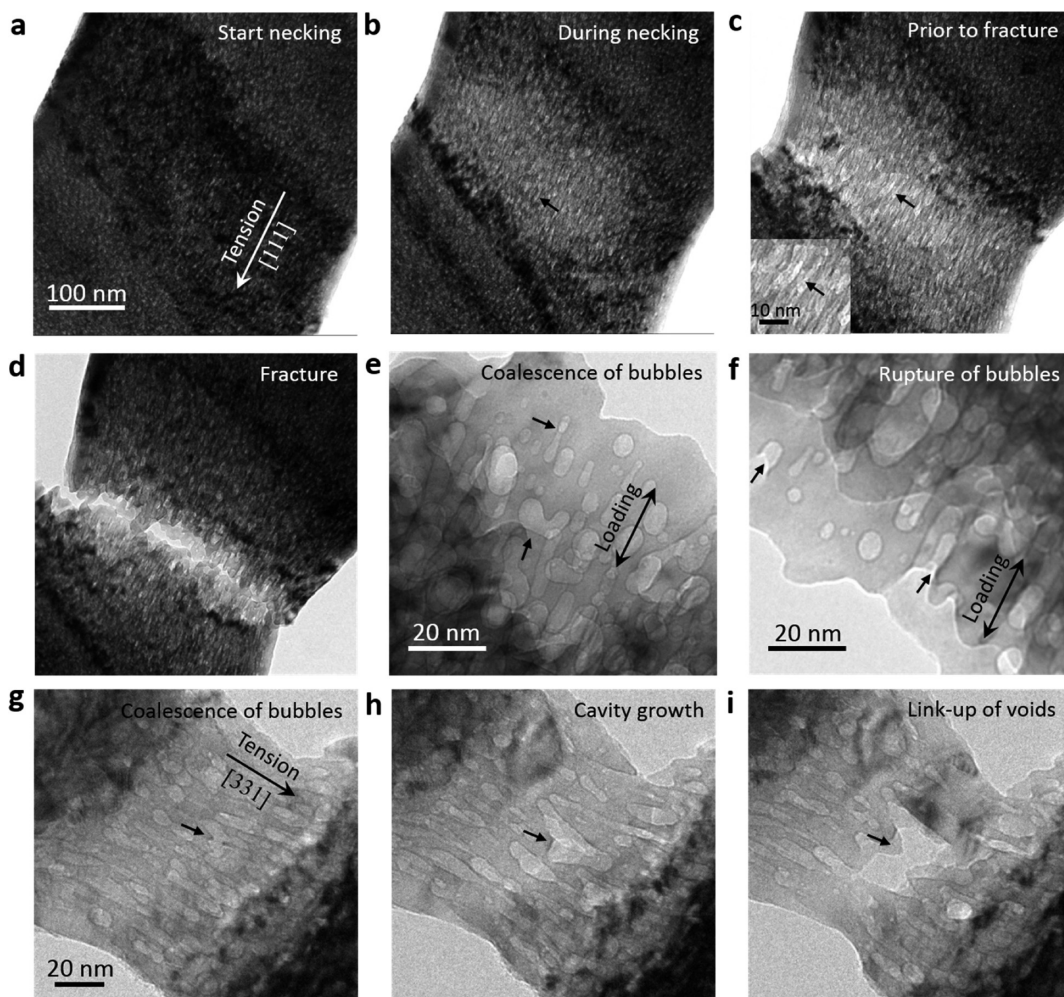


Figure 3. Necking deformation of the nano bubbled Cu single crystal pillar. (a) Image of the nanoscale NB-Cu at the point right before necking. Loading axis is near [111]. The white dots are the typical under-focus images of numerous He bubbles. (b–d) Details of deformation of He bubbles and Cu nanoligaments during necking. Panels b–d have the same scale bar as a. (e and f) Deformed bubbles near fracture surface in the failed NB-Cu single crystal in a. (g–i) Failure of NB-Cu via He bubbles growth and coalescence observed in a sample loaded along [331].

c show the typical transmission electron microscopy (TEM) image of the He-implanted Cu, and Figure 1d is the corresponding illustration of the microstructures, hereon called nano bubbled Cu (NB-Cu). The He bubbles have diameter d of several nanometers and a peak distributed around $\langle d \rangle = 6.6$ nm, which are larger than the He bubbles formed by room temperature implantation in previous studies,^{16–20} thus is more convenient to track the deformation of He bubbles during in situ loading. They are nearly spherical instead of faceted, indicating internal He pressurization. The He pressure for equilibrium bubbles can be estimated from the Young–Laplace equation $P_{\text{bubble}} \approx 4\gamma_s/d \approx 1$ GPa, where $\gamma_s = 2.12$ J/m² is the surface energy of Cu.²³ The total volume fraction of the He bubbles is around 10% in NB-Cu samples, see details in Supporting Information (SI) and Figure S1. A high-resolution TEM image (Figure 1c) reveals no visible defects around the bubbles before the deformation.

We then performed systematic in situ mechanical tests inside a TEM (more details in SI) with 10 NB-Cu samples and 10 fully dense Cu (FD-Cu) samples as control, of diameter D in the range of 93–301 nm (Table S1). Figure 2a–d shows the typical compressive behaviors of NB-Cu vs FD-Cu. For FD-Cu pillar with $D = 170$ nm, under compressing along [751]

direction, it exhibits yielding around 700 MPa, followed by a series of strain bursts as shown by the blue stress–strain curve in Figure 2d, indicating unstable plasticity.^{1–9} The intermittent strain bursts are usually accompanied by sharp slip bands, as shown in Figure 2b and Figure S2a. In contrast, the NB-Cu pillar with the same D , when compressed along the same direction, demonstrates higher yield strength (≈ 940 MPa)^{16,17} and more stable stress–strain response as displayed by the red curve in Figure 2d. Upon yielding, the NB-Cu pillar deforms homogeneously and forms a rather smooth surface profile instead of sharp slip steps, as marked in Figure 2c and Figure S2b.

In situ tensile tests were also conducted, as shown in Figures 2e–g. Similar to compression, the FD-Cu pillar with [311] orientation and $D = 200$ nm shows lower yield strength (≈ 400 MPa), frequent strain bursts, and the formation of surface slip steps, as marked in Figure 2e. In contrast, the NB-Cu pillar with [311] orientation and similar D has a much higher yield strength (≈ 800 MPa), relatively stable stress–strain flow, and slight work hardening after yielding under tensile loading, as shown by the true stress–strain curve in Figure 2g. With such more stable and controllable stress–strain response in NB-Cu, a short uniform deformation stage can be identified, followed

by a long necking deformation stage, as displayed in Figures 2f–g, Figure S3, and Movie S1. In tension, this NB-Cu pillar has $\approx 3.5\%$ uniform plastic elongation and shows slight work hardening after yielding in true stress–true strain curve (see Figure 2g and Figure S3). The total elongation of 17% at final ductile fracture is much larger than that of the nanoporous gold (NPG) sample having an open porous structure.^{24–27} It suggests that closed sub-10 nm bubbles are better at maintaining continuous controllable plastic deformation. It is quite different from the radiation-induced He embrittlement of bulk polycrystalline materials, where He tends to concentrate along 2D grain boundaries.^{10–14} The reason for it in the case of submicron-sized materials will be fully discussed later. Similar results were also evidenced by compressive and tensile tests under different loading directions, summarized in Figure S4 and Table S1. All of the NB-Cu samples with D between 93 and 301 nm achieved a reduction of area of more than 40% (Figure S5), indicating that submicron-sized NB-Cu is ductile indeed.

By quantitative load–displacement and sample profile measurements, NB-Cu demonstrates both uniform deformation and necking stages (Figure 2 and Figure S3). Figure 3a–f shows the detailed necking deformation of a NB-Cu pillar loaded along $[111]$ direction. As the sample gets thinner, the deformation is finally localized to a 200 nm wide region as the darker contrast area in Figure 3a, and individual He bubbles become visible in TEM. As deformation proceeded, the He bubbles (white dots) were stretched extensively (Figure 3b). At the point just prior to the final fracture, several larger cavities from the growth and coalescence of bubbles can be identified, as marked by the black arrows and highlighted as an inset in Figure 3c. Further straining made the sample fracture rapidly with serrated fracture surface almost perpendicular to the loading axis, as displayed in Figure 3d.

He bubbles in the neck region were elongated significantly and demonstrated local super deformability until the final fracture. The final fracture was caused by the bubble growth and coalescence (Figures 3e and f), and once the coalesced size became larger than a critical value,²⁸ locally ductile rupture of the sample occurred very rapidly. Notably, the experiment was conducted inside the TEM, which allowed us to capture the features of the crack fronts just after failure. In the region near the fracture surfaces (Figure 3e and f), bubbles were deformed from the original aspect ratio of 1:1 to 1:3, and some even to 1:6. Other bubbles were also coalescing with the adjacent ones, but this ceased suddenly due to unloading caused by failure, as revealed by the “w” shape of bubble edge in Figure 3e. After fracture, a large number of elongated and ruptured bubbles are formed near the fracture surface, as highlighted in Figures 3e and f. The detailed necking deformation is shown in Movies S2. The fracture processes resulting from the growth and coalescence of He bubbles for a thinner sample loaded along $[331]$ are displayed in Figure 3g–i. After the deforming bubbles coalesce (Figure 3g), the stress level around the cavity is enhanced significantly due to load shedding, thus further accelerating the localized deformation (Figure 3h), and leading to quickly rupture of the sample (Figure 3i). The significant growth and coalescence of bubbles are the critical event for the severe plastic localization and final failure. Overall, the NB-Cu showed a ductile deformation, before significant bubble growth and coalescence, then there is the transition to sudden rupture.

As the He bubbles serve as 3D fiducial markers, we performed more in situ bending tests with a prefabricated notch, to unveil the detailed plasticity as shown in Figure 4a

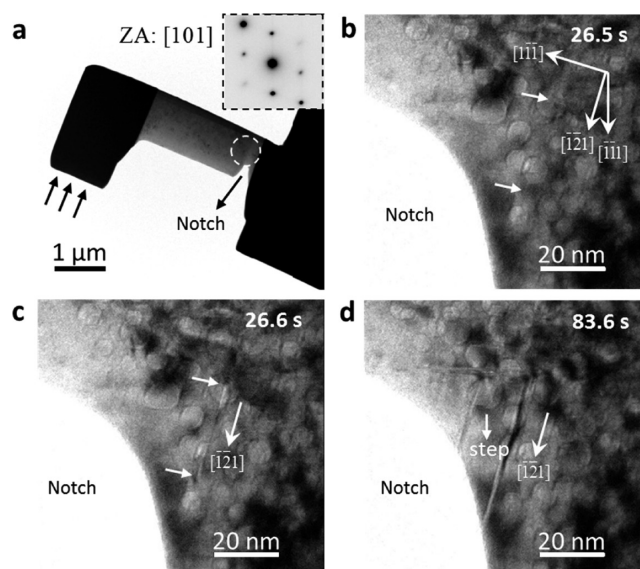


Figure 4. In situ bending test reveals the emission of dislocations from He bubbles. (a) Geometry of the NB-Cu sample used for in situ bending test. (b and c) Extracted images showing a partial dislocation nucleate from the He bubble within 0.1 s and cut through several He bubbles during propagation, and finally a stacking fault is formed behind. (d) A typical slip step is formed on the bubble surface.

and Movie S3. Such tests have several advantages: First, the deformation under bending is mainly initiated at the notch region, and it is thus easier to capture the initial plasticity; Second, as loading proceeds, the notch region becomes thinner, which is better for high quality image recording; As shown in Figure 4b–c, the nucleation of dislocations and the bubble–dislocation interactions can be captured. Two likely steps of deformation are suggested based on Figure 4 and Movie S3: First, dislocation emissions are most likely from the interior of the sample, in particular the internal surfaces of He bubbles (Figure 4c), instead of from the sample’s exterior surfaces, which means He bubbles are likely the dominant dislocation source in NB-Cu; Second, once a partial dislocation is nucleated, it can slip along the (111) plane and cut through the He bubbles, thus small slip steps are created on the bubbles surface, as evidenced by the stacking faults and steps marked in Figure 4c and d. Movie S4 shows another high magnification video of the compression behavior of a NB-Cu pillar. It is suggested that dislocations also prefer to nucleate from the He-facing surfaces, besides some dislocations nucleated from the pillar top due to stress concentration, hence both internal and external dislocation sources are activated simultaneously. In contrast to the high-speed escape of dislocations in FD-Cu pillar, the propagation of dislocations in NB-Cu are seen to be highly limited by the He bubbles.

The systematic experiments above indicated that submicron-sized NB-Cu has higher yield strength, relatively stable plastic flow, slight work hardening and uniform deformation stage (Figure 2g and S3), which are superior to strain-burst dominated plasticity of single crystal pillars^{1–9} and the brittle fracture of NPG.^{24–27} For better understanding of the elementary defect processes, atomistic simulations were performed (details can be found in SI). The calculations indicated that dislocations are preferentially nucleated from the He-facing surfaces at the resolved shear stress levels above ≈ 1.5 GPa, which are required for frequent dislocation nucleation

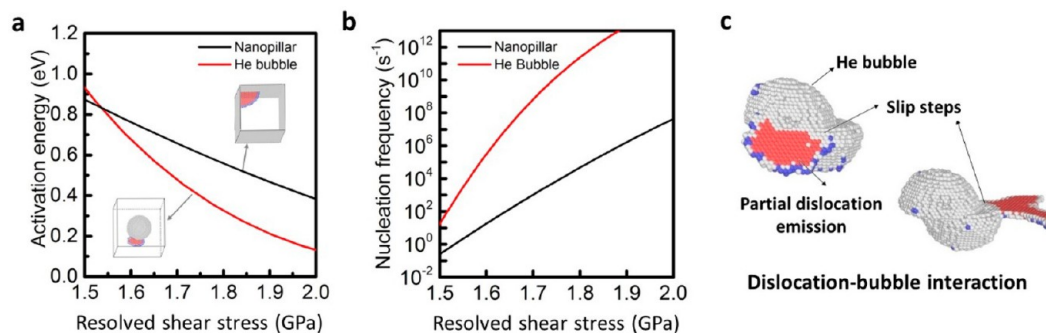


Figure 5. Atomistic calculations further prove He bubbles are preferential dislocation sources. (a) The activation energy for dislocation nucleation from He bubbles is lower than that from the corner of a nanopillar. (b) The nucleation frequency of dislocations from He bubbles is higher than that from the corner of a nanopillar. (c) He bubble and the newly formed slip steps on bubble surface are active dislocation sources during further straining.

within the usual testing time of seconds. At these stress levels, computed activation energy of dislocation nucleation from He bubble is slightly lower (Figure 5a) and the nucleation frequency is higher than that from the corner of nanopillar (Figure 5b). Therefore, He bubbles are more active dislocation sources than the nanopillar surface/corner. Furthermore, dislocation-bubble interactions can lead to the higher shear strength²⁹ and more internal obstacles, thus decreasing the mean free path of dislocation compared to the He-free pillar and induce more dislocation storage (Figure 2 and S7). According to the strain-hardening models, the increment of shear stress during plastic deformation is mainly the results of the dislocation storage,³⁰ such as $\frac{d\tau}{d\gamma} \propto \frac{d\rho}{d\gamma} = \frac{1}{bL}$, where b is the Burgers vector and L is the mean free path of dislocations. During the plastic deformation of NB-Cu, several factors are leading to the shortening of the mean free path (L) of dislocations: (1) High-density internal He bubbles are obstacles for dislocation slip, and their average spacing is only ~ 15.6 nm, which is much smaller than L in FD-Cu pillar ($\approx D$), thus more dislocations can be stored in NB-Cu under deformation; (2) numerous He bubbles are dislocation sources, so more dislocations can be triggered at the same time, and frequent dislocation interactions and reactions further reduce L . The hardening may also be contributed by the reduced metal ligament/wall size that the dislocation needs to pass through in order to have percolating plasticity. The mechanisms discussed above contributed to the slight strain hardening and more stable and homogeneous deformation of NB-Cu under tensile loading. However, the strain hardening ability of NB-Cu is still very limited, thus strain localization (necking) sets in (Figures 2g and S3) quickly after very short uniform deformation stage.

In NB-Cu we see that before the significant growth and coalescence of bubbles, the whole sample actually deforms quite stable and ductile. Previous experiments have already revealed the presence of grain boundaries, interfaces, or precipitates would improve the controllability of plastic deformation in small-volume crystals because they limit the mean free path of freshly nucleated dislocations, preventing dislocation avalanches.^{4,31–34} We expect the sub-10 nm He bubbles will do the same of limiting dislocation velocity and mean free path, thus producing more diffuse deformation.^{15–20} But, once the bubbles grow too much and link up to reach a critical size,²⁸ failure nearly 90° to the tensile axis (Figure 3d and i) will likely proceed rapidly. Even then, the metals deform plastically, as evidenced by the severely stretched nanoliga-

ments; at no point do we see true atomic-scale brittle fracture like in many ceramics materials at room temperature.³⁵

If we identify significant bubble growth and coalescence as the watershed event between controllable deformation and uncontrollable failure, the size effect on ductility can be explained by Weibull statistics, even though we are not dealing with ceramics. In a bulk metal, it is highly possible due to pre-existing defects that several bubbles already linked up before deformation. Indeed, we know He bubbles preferentially accumulate along grain boundaries; hence the He cavity may easily exceed the critical size in irradiated bulk polycrystals.^{10–14} In that case, failure would happen immediately upon tensile straining along a preferentially oriented grain boundary. If we do have a single crystal without any pre-existing defects except for closed, perfectly spherical nanoscale bubbles, we can then assume that with application of plastic strain $\epsilon_{\text{tensile}}$ and the resultant more or less predictable bubble shape change, the probability that there are several bubbles linking up is $dVf(\epsilon_{\text{tensile}})$, where dV is the volume element under consideration and $f(\epsilon_{\text{tensile}})$ is a monotonically increasing damage function that may be modeled by a power-law $f(\epsilon_{\text{tensile}}) = (\epsilon_{\text{tensile}}/\epsilon_0)^m$. We expect to lose control when the probability of finding one critical sized flaw in the whole sample of volume V , $1 - \exp(-Vf(\epsilon_{\text{tensile}}))$, reaches order 1, which leads to a controllable strain range $\epsilon_{\text{tensile}}$ that scales as $V^{-1/m}$, that tends to 0 as $V \rightarrow \infty$. In other words, for infinite-volume sample, we expect the controllable plastic strain limit is zero, and catastrophic fracture nearly 90° to the tensile axis should happen immediately, because there is always locations with critical-sized cavity that reduced the bonded area and markedly enhanced local stress, thus promoting localized cracking. On the other hand, if the volume is finite, then the controllable strain range can be significant, which explains the ductility of submicron-sized NB-Cu. This argument can also explain why the nanoporous gold appears to be more brittle even in small-volume samples, this is because their open pores have much larger size and volume fraction.^{24–27} In NB-Cu, the nanoscale He bubbles are isolated from each other and less vulnerable to stress concentration²⁸ and have good initial stability during plastic deformation.

Finally, the roles of bubble pressure on the plasticity and fracture of NB-Cu need to be discussed. Due to He pressurization, the bubbles tend to form spherical shape rather than the faceted cavities or interconnected cavities. In addition, atomistic calculations show that the bubble pressure plays an important role. For a He bubbles with pressure of 1 GPa,

dislocation can cut through the bubbles but the critical stress for dislocation slip is higher than that in a single crystal (Figure 4 and S7). But for similarly sized He bubbles with $P_{\text{bubble}} = 7$ GPa (performed by MD simulations to reflect the general trend of the effect of bubble pressure), they can block the slip of dislocations, and lead to cross slip or activate new dislocations on bubble surface along other slip planes (Movie S5). Lastly, for the loading rate (strain rate $\approx 10^{-3}$ /s) used in this study, surface diffusion does not appear to play a critical role in the plastic deformation but could play a role in smoothing the surface once a fracture surface has been created (Figures 3e and f).

In summary, nano bubbled copper (NB-Cu) can be fabricated by high-temperature He ion implantation. Systematic in situ compressive and tensile tests demonstrated that submicrometer-sized NB-Cu samples (100–300 nm) shows more controllable and ductile deformation due to the numerous embedded sub-10 nm He bubbles, which increase dislocation storage and reduce dislocation velocity and mean free path. Such He bubbles enhanced ductility can be rationalized on the basis of He bubbles serving as regulator of plasticity and the relative tolerance of nanoscale flaws due to Weibull statistics. The new concept of ‘radiation enhanced ductility’ and nano bubbled metals could open up new avenues for making more mechanically robust nano- and micro-structures by He bubble engineering. As an unexpected side product of this research, our experimental protocol of tracking the shapes and sizes of sparsely implanted He bubbles could be a powerful technique for resolving 3D plastic strain and damage distribution close to the fracture singularity.

■ ASSOCIATED CONTENT

Supporting Information

The Supporting Information is available free of charge on the ACS Publications website at DOI: 10.1021/acs.nanolett.6b00864.

A brief statement for the sample preparation and details and in situ TEM testing (PDF)

Tension test on the NB-Cu sample (AVI)

Necking deformation of the NB-Cu sample (AVI)

Bending test on the NB-Cu pillar (AVI)

Compression test on the NB-Cu pillar (AVI)

An edge dislocation interacts with a He bubble with 7 GPa internal pressure (AVI)

■ AUTHOR INFORMATION

Corresponding Authors

* E-mail: wzhanxjtu@mail.xjtu.edu.cn.

* E-mail: liju@mit.edu.

Notes

The authors declare no competing financial interest.

■ ACKNOWLEDGMENTS

This work was supported by the National Natural Science Foundation of China (Grant Nos. 51471128, 51231005, 51321003). W.Z.H. would like to thank the support of Youth Thousand Talents Program of China and the Young Talent Support Plan of XJTU. S.O. acknowledges support by ESISM Japan and JSPS KAKENHI (Grant Nos. 22102003, 23246025, and 25630013). J.L. acknowledges support by NSF DMR-1410636 and DMR-1120901. W.Z.H. acknowledges the assistance of E.G.F and Y.Q.W in ion implantation.

■ REFERENCES

- (1) Zhu, T.; Li, J. Ultra-Strength Materials. *Prog. Mater. Sci.* **2010**, *55*, 710–757.
- (2) Dimiduk, D. M.; Woodward, C.; LeSar, R.; Uchic, M. D. Scale-Free Intermittent Flow in Crystal Plasticity. *Science* **2006**, *312*, 1188–1190.
- (3) Csikor, F. F.; Motz, C.; Weygand, D.; Zaiser, M.; Zapperi, S. Dislocation Avalanches, Strain Bursts, and the Problem of Plastic Forming at the Micrometer Scale. *Science* **2007**, *318*, 251–254.
- (4) Uchic, M. D.; Dimiduk, D. M.; Florando, J. N.; Nix, W. D. Sample Dimensions Influence Strength and Crystal Plasticity. *Science* **2004**, *305*, 986–989.
- (5) Greer, J. R.; Oliver, W. C.; Nix, W. D. Size Dependence of Mechanical Properties of Gold at the Micro Scale in the Absence of Strain Gradients. *Acta Mater.* **2005**, *53*, 1821–1830.
- (6) Shan, Z. W.; Mishra, R. K.; Syed Asif, S. A.; Warren, O. L.; Minor, A. M. Mechanical Annealing and Source-limited Deformation in Submicrometre-Diameter Ni Crystals. *Nat. Mater.* **2008**, *7*, 115–119.
- (7) Yu, Q.; Shan, Z. W.; Li, J.; Huang, X. X.; Xiao, L.; Sun, J.; Ma, E. Strong Crystal Size Effect on Deformation Twinning. *Nature* **2010**, *463*, 335–338.
- (8) Greer, J. R.; De Hosson, J. T. M. Plasticity in Small-Sized Metallic Systems: Intrinsic Versus Extrinsic Size Effect. *Prog. Mater. Sci.* **2011**, *56*, 654–724.
- (9) Wang, Z. J.; Shan, Z. W.; Li, J.; Sun, J.; Ma, E. An Index for Deformation Controllability of Small-Volume Materials. *Sci. China: Technol. Sci.* **2014**, *57*, 663–670.
- (10) Nastasi, M.; Mayer, J. W.; Hirvonen, J. K. *Ion-Solid Interactions: Fundamentals and Applications*; Cambridge University Press, 1996.
- (11) Kramer, D.; Brager, H. R.; Rhodes, C. G.; Pard, A. G. Helium Embrittlement in Type 304 Stainless Steel. *J. Nucl. Mater.* **1968**, *25*, 121–131.
- (12) Ullmaier, H. Helium in Fusion Materials-high Temperature Embrittlement. *J. Nucl. Mater.* **1985**, *133*, 100–104.
- (13) Trinkaus, H.; Singh, B. N. Helium Accumulation in Metals During Irradiation-Where Do We Stand? *J. Nucl. Mater.* **2003**, *323*, 229–242.
- (14) Han, W. Z.; Demkowicz, M. J.; Mara, N. A.; Fu, E. G.; Sinha, S.; Rollett, A. D.; Wang, Y. Q.; Carpenter, J. S.; Beyerlein, I. J.; Misra, A. Design of Radiation Tolerant Materials via Interface Engineering. *Adv. Mater.* **2013**, *25*, 6975–6979.
- (15) Kiener, D.; Hosemann, P.; Maloy, S. A.; Minor, A. M. In Situ Nanocompression Testing of Irradiated Copper. *Nat. Mater.* **2011**, *10*, 608–613.
- (16) Li, N.; Mara, N. A.; Wang, Y.; Nastasi, M.; Misra, A. Compressive Flow Behavior of Cu Thin Films and Cu/Nb Multilayers Containing Nanometer-scale Helium Bubbles. *Scr. Mater.* **2011**, *64*, 974–977.
- (17) Guo, Q.; Landau, P. L.; Hosemann, P.; Wang, Y.; Greer, J. R. Helium Implantation Effects on the Compressive Response of Cu Nanopillars. *Small* **2013**, *9*, 691–696.
- (18) Landau, P.; Guo, Q.; Hattar, K.; Greer, J. R. The Effect of He Implantation on the Tensile Properties and Microstructure of Cu/Fe Nano-Bicrystals. *Adv. Funct. Mater.* **2013**, *23*, 1281–1288.
- (19) Lontas, R.; Gu, X. W.; Fu, E. G.; Wang, Y. Q.; Li, N.; Mara, N.; Greer, J. R. Effects of Helium Implantation on the Tensile Properties and Microstructure of Ni₇₃P₂₇ Metallic Glass Nanostructures. *Nano Lett.* **2014**, *14*, 5176–5183.
- (20) Miura, T.; Fujii, K.; Fukuya, K. Micro-Mechanical Investigation for Effects of Helium on Grain Boundary Fracture of Austenitic Stainless Steel. *J. Nucl. Mater.* **2015**, *457*, 279–290.
- (21) Han, W. Z.; Demkowicz, M. J.; Fu, E. G.; Wang, Y. Q.; Misra, A. Effect of Grain Boundary Character on Sink Efficiency. *Acta Mater.* **2012**, *60*, 6341–6351.
- (22) Ziegler, J. F.; Biersack, J. P.; Littmark, U. *The Stopping and Range of Ions in Solids*; Pergamon Press: New York, 1985.
- (23) Li, N.; Nastasi, M.; Misra, A. Defect Structures and Hardening Mechanism in High Dose Helium Ion Implanted Cu and Cu/Nb Multilayer Thin Films. *Int. J. Plast.* **2012**, *32–33*, 1–16.

- (24) Li, R.; Sieradzki, K. Ductile-Brittle Transition in Random Porous Au. *Phys. Rev. Lett.* **1992**, *68*, 1168–1171.
- (25) Biener, J.; Hodge, A. M.; Hamza, A. V. Microscopic Failure Behavior of Nanoporous Gold. *Appl. Phys. Lett.* **2005**, *87*, 121908.
- (26) Lee, D. Y.; Wei, X. D.; Chen, X.; Zhao, M. H.; Jun, S. C.; Hone, J.; Herbert, E. G.; Oliver, W. C.; Kysar, J. W. Microfabrication and Mechanical Properties of Nanoporous Gold at the Nanoscale. *Scr. Mater.* **2007**, *56*, 437–440.
- (27) Balk, T. J.; Eberl, C.; Sun, Y.; Hemker, K. J.; Gianola, D. S. Tensile and Compressive Microspecimen Testing of Bulk Nanoporous Gold. *JOM* **2009**, *61*, 26–31.
- (28) Gao, H. J.; Ji, B. H.; Jager, I. L.; Arzt, E.; Fratzl, P. Materials Become Insensitive to Flaws at Nanoscale: Lessons from Nature. *Proc. Natl. Acad. Sci. U. S. A.* **2003**, *100*, 5597–5600.
- (29) Wei, Q. M.; Li, N.; Mara, N.; Nastasi, M.; Misra, A. Suppression of Irradiation Hardening in Nanoscale V/Ag Multilayers. *Acta Mater.* **2011**, *59*, 6331–6340.
- (30) Devincere, B.; Hoc, T.; Kubin, L. Dislocation Mean Free Paths and Strain Hardening of Crystals. *Science* **2008**, *320*, 1745–1748.
- (31) Mara, N. A.; Bhattacharyya, D.; Dickerson, P.; Hoagland, R. G.; Misra, A. Deformability of Ultrahigh Strength 5 nm Cu/Nb Nanolayered Composites. *Appl. Phys. Lett.* **2008**, *92*, 231901.
- (32) Zhang, J. Y.; Liu, G.; Lei, S. Y.; Niu, J. J.; Sun, J. Transition from Homogeneous-Like to Shear Band Deformation in Nanolayered Crystalline Cu/Amorphous Cu-Zr Micropillars: Intrinsic vs. Extrinsic Size Effect. *Acta Mater.* **2012**, *60*, 7183–7196.
- (33) Jang, D. C.; Li, X. Y.; Gao, H. J.; Greer, J. R. Deformation Mechanisms in Nanotwinned Metal Nanopillars. *Nat. Nanotechnol.* **2012**, *7*, 594–601.
- (34) Gu, R.; Ngan, A. H. W. Size Effect on the Deformation Behavior of Duralumin Micropillars. *Scr. Mater.* **2013**, *68*, 861–864.
- (35) Zhu, T.; Li, J.; Yip, S. Atomistic Characterization of Three-Dimensional Lattice Trapping Barriers to Brittle Fracture. *Proc. R. Soc. London, Ser. A* **2006**, *462*, 1741–1761.